



Effect of a novel controlled thermomechanical treatment on the microstructure and mechanical properties of a high-carbon nanobainitic steel

K. Janus¹ · L. Rogal^{1,2} · J. Dutkiewicz¹ · R. Chulist¹ · G. Korpala³ · U. Prah³ · K. Konczak² · P. Kochmanski⁴ · K. Nalepka⁵ · W. Maziarz¹

Received: 30 May 2023 / Revised: 18 August 2023 / Accepted: 23 September 2023 / Published online: 21 October 2023
© The Author(s) 2023

Abstract

The effect of the novel controlled thermomechanical treatment, including torsion components in the elastic strain range during the isothermal holding on the microstructure and mechanical properties of the high-carbon nanobainitic steel, was investigated. TEM observations of the thermo-mechanically treated steel revealed bainitic ferrite laths with an average size of 68 ± 40 nm and films of retained austenite with an average size of 34 ± 17 nm, along with the blocky morphology of retained austenite in sub-micron scale. The XRD synchrotron diffraction allows estimating the amount of retained austenite at $43.1 \pm 1.2\%$ volume fraction with a carbon concentration of 1.17 ± 0.09 wt.%. Furthermore, the deconvolution of (200) Fe- γ reflections corresponding to two different low-carbon and high-carbon retained austenite peaks and, simultaneously, the blocky and film-like retained austenite was performed. In addition, the Nishiyama–Wassermann (N–W) crystallographic orientation relationship between bainitic ferrite and retained austenite was described as dominant using the misorientation distribution function (MDF). The crystallographic texture results indicated that the main growth of bainitic ferrite plates occurred after removing external stress during isothermal holding. The tensile tests and hardness measurements showed a high tensile strength achieved mainly by nano-metric bainitic ferrite plates and a high dislocation density. The high level of elongation is most likely attained due to a high amount of retained austenite in steel and both TRIP and TWIP effects during tensile deformation.

Keywords Stress-induced bainitic transformation · Microstructure · Mechanical properties · TRIP and TWIP effects · High-carbon nanobainitic steel

1 Introduction

The carbide-free bainitic (CFB) steel represents the 3rd generation of advanced high-strength steels (AHSSs) with a low alloying element content and the transformation-induced plasticity (TRIP) effect during deformation [1]. The typical microstructure of CFB steel consists of very fine bainitic ferrite plates (α_{BF}) and austenitic films (γ_f) or blocky types of retained austenite (γ_b) in the volume fraction range between 20 and 50% [2]. In this context, the distribution of carbon is controlled by alloying the steel with Si and/or Al. In the case of nanostructured bainitic steel, a minimum silicon content close to 1.5 wt.% is required to suppress the cementite precipitation. Aluminum exhibits a similar effect just if the Si and Al content is balanced. This, in turn, allows for achieving carbon-enriched austenite [1, 3]. On the other hand, some contributions, such as Qian and co-workers

✉ K. Janus
k.janus@imim.pl

¹ Institute of Metallurgy and Materials Science, Polish Academy of Sciences, Reymonta 25 Str., 30 059 Krakow, Poland

² Gonar Bis, Obroki 109 Str., 40-833 Katowice, Poland

³ Institut für Metallformung, TU Bergakademie Freiberg, Bernhard-von-Cotta-Straße 4, 09596 Freiberg, Germany

⁴ Faculty of Mechanical Engineering and Mechatronics, West Pomeranian University of Technology in Szczecin, al. Piastów 19, 70-310 Szczecin, Poland

⁵ Faculty of Mechanical Engineering and Robotics, AGH University of Science and Technology, al. Adama Mickiewicza 30, 32-250 Krakow, Poland

[4], dealing with carbide-free bainitic steel microstructure, report a small fraction of martensite, which indicates sluggish carbon transfer. In light of the above, a whole spectrum of microstructures in CFB can be obtained depending on the treatment conditions. For instance, a good combination of the ultimate tensile strength (UTS) at approximately 2.2 GPa, hardness values of about 600–670 HV, uniform elongation in the range of 5–30%, and a good toughness up to 130 MPa m^{1/2} is reported in [5, 6]. Such mechanical properties provide a wide application of the advanced CFB steels, e.g., in the defense industry (as armor elements), mining industry (as elements with high abrasive wear resistance), and in the aerospace industry (as elements of an aircraft landing gear), or in the bearing industry [7, 8]. However, to obtain the nanobainitic microstructure with excellent mechanical properties, isothermal heat treatment has to be carried out at very low temperatures ranging between 125 °C and 325 °C. Nevertheless, from an economic point of view, this temperature should not exceed 200 °C. To perform a complete bainitic transformation, the steel needs a very long treatment time, reaching even a few hours or days [9, 10]. One of the first high-carbon nanobainitic steels, which achieved a hardness of 600 HV, was isothermally held at 200 °C for 9 days [11]. In the case of another high-carbon nanobainitic steel, the modification of chemical compositions by adding the boron or titanium did not shorten the total time of bainitic transformation. In both cases, the time needed to complete bainitic transformation was more than 9 days [12, 13]. Therefore, economic and ecological factors require the acceleration of the kinetics of bainitic transformation, thereby reducing the total time needed to obtain the nanobainitic microstructure. In this context, the main effort of further research on high-carbon nanobainitic steel is to find a process that shortens the bainitic transformation time. In recent years, many research papers have utilized such methods since can accelerate the kinetics of bainitic transformation. First, the kinetics of bainitic transformation can be accelerated by refining the grain size of parent austenite. Refined austenite grains increase the density of nucleation sites for bainitic ferrite and accelerate its nucleation [14]. This phenomenon leads to the formation of the nanostructured bainitic steel with a hardness of 625 HV, UTS of 2154 MPa, and elongation at 13.0%, simultaneously decreasing the isothermal holding time to 24 h at 220 °C following austenitization at 1000 °C for 30 min [15]. The quenching to martensite is the next applied procedure accelerating the kinetics of the bainitic transformation of high-carbon nanobainitic steel, followed by a low-temperature isothermal bainitic transformation [16]. The generation of dislocations near the martensite/austenite interfaces leads to a higher frequency of nucleation sites for the bainitic ferrite plates and decreases the nanobainitic transformation time [16, 17]. However, two of the most perspective methods to accelerate the kinetics

of bainitic transformation are related to chemical (ΔG_{chem}) and mechanical (ΔG_{mech}) driving forces. The first, which increases the chemical driving force of bainitic transformation and refines the austenite grains, relies on introducing the alloying elements such as Al, Co, or both to a solid solution. Such an approach causes a shorter isothermal holding time, i.e., about 78 h at 200 °C in the case of high-carbon nanobainitic steel [18, 19]. The latter includes the application of external stress or strain during isothermal heat treatment leading to a drastic decrease in isothermal heat treatment time by increasing the mechanical driving force of bainitic transformation. This method is also referred to as stress-induced or strain-induced transformation [20, 21]. In a situation where the additional stress was applied to the steel during bainitic transformation, the total driving force of the system ($\Delta G^{\gamma \rightarrow \alpha}$) can be decomposed into the ΔG_{chem} and ΔG_{mech} , where ΔG_{mech} is defined in Eq. 1 [22]:

$$\Delta G_{\text{mech}} = \sigma_N \zeta + \tau s \quad (1)$$

where σ_N is the normal stress on the habit plane, τ is the shear stress component on the habit plane, ζ is the dilatation component of the shape deformation (0.03), and s is the shear component of the shape deformation (0.26). In Ref. [23], the authors indicated that the high-carbon nanobainitic steel can be obtained by applying additional compressive stress during bainitic transformation due to an increase in the rate of bainite nucleation. In addition, introducing the additional mechanical driving force increases the bainite start temperature and simultaneously accelerates the kinetic of bainitic transformation [24]. The external stress can be applied above or below the yield strength of austenite (σ_y) that corresponds to plastic strain or elastic deformation, respectively. Large deformation can delay the bainitic transformation by forming mechanically stabilized austenite [23, 25]. In contrast, the stress in the elastic range accelerates the kinetics of bainite transformation, mainly by growing the bainitic ferrite plates. Furthermore, it can suppress or eliminate cementite precipitations. Moreover, the employment of the external stress to austenite (below the yield strength of austenite) is very effective at the extremely low bainitic transformation temperature i.e., just above the martensitic start temperature (M_s). In these conditions, the bainitic transformation is suddenly accelerated, mainly in the early stages of austenite decompositions [26–29]. The role of elastic stress in the nanobainitic transformation in the case of high-carbon bainitic steel has been described in Ref. [23]. The authors emphasize that the additional elastic stress (compressive uniaxial stress) during bainitic transformation increases the bainitic start temperature and accelerates the transformation due to the growth of compliant variants, leading to an organized microstructure. Another effect of external stress application is variant selections that favored the

growth of specific crystallographic orientations of bainite. This is especially the case for the stresses below the yield stress of austenite [30, 31]. This in turn produces anisotropic plastic bainite deformation (transformation plasticity (TP)). The effect increases with the magnitude of external stress and results in anisotropic volume change [32, 33]. The development of microstructure upon TP strain is explained by Magee [34] and Greenwood-Johnson [35]. To summarize, applying additional stress before the bainitic reaction and after austenitization can shorten the time needed to obtain the nanostructured bainitic steel even down to 90 min [28, 36].

Although several types of research indicated that the potential of strain-induced bainitic transformation in the context of a high-carbon nanobainitic steel, the actual knowledge of the influence of external elastic deformation causing the acceleration of the bainitic transformation kinetics (stress-induced bainitic transformation), especially in the case of shear stress and high-carbon nanobainitic steel required complementation. Therefore, the main aim of this study is to determine the influence of elastic stress using torsion deformation during the first stage of isothermal heat treatment on the microstructure and mechanical properties of high-carbon nanobainitic steel obtained by the novel controlled thermomechanical treatment.

2 Materials and methods

2.1 Material manufacturing

The high-carbon nanobainitic steel was supplied as a bar of 80 mm in diameter. The chemical composition of experimental steel is Fe–0.78C–1.67Si–2.45Mn–1.35Cr–0.21Mo–1.30Al (all in wt. %). The thermomechanical treatment process consists of homogenization at 1250 °C and hot-rolling during austenitization, where the minimum rolling temperature was 950 °C. Before being slowly cooled to room temperature into the air, the sample was rapidly cooled to bainitic transformation temperature using water under pressure, obtaining an average Prior Austenite Grain (PAG) size of 12 ± 2 μm . Next, 30 s after reaching the bainitic transformation temperature of 200 °C, the external stress below the yield strength of parent austenite (250 MPa) was applied to the steel for 10 s and then cooled to 190 °C, where the sample was held for 30 min to obtain the nanobainitic microstructure Fig. 1. The σ_y was determined in the torsion test. During this test, after the austenitization at 950 °C for 5 min and rapid cooling to the bainitic transformation temperature of 200 °C and holding for 30 s, the maximum torsion stress generated by the simulator was applied. In this way, the torque relationship in the function of the twist angle was plotted. Based on this, using a Huber–Mises–Hencky

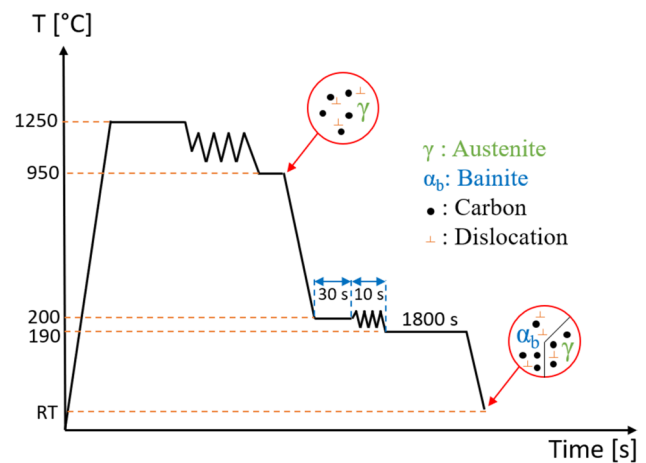


Fig. 1 The thermomechanical treatment procedure employed to manufacture the high-carbon nanobainitic steel

criterion, the equivalent stress–strain curve was determined, and the 0.2% proof strength was 438 MPa. According to the literature [26], the stress used to induce the bainitic transformation was estimated at 250 MPa as the 60% of yield strength of parent austenite to avoid significant plastic deformation during isothermal holding.

2.2 Material characterization

Optical observations of the samples were performed using a Leica DMIRM light optical microscope (LOM). For this purpose, the samples were initially ground, polished on silica suspension, and finally etched in 4% Nital. The thermal etching [37], in conjunction with LOM micrographs and ImageJ software, was carried out to reveal the PAG size. More detailed microstructure observations were carried out using scanning electron microscopes (SEM) FEI E-SEM XL 30. Samples for SEM observations were polished on silica suspension and etched in 4% Nital by 15 s. Secondary electron (SE) and backscatter electron (BSE) detectors in Z-contrast were used with an accelerating voltage of 20 kV. The FEI Quanta 3D 200i FEG-SEM microscope was also used for electron backscatter diffraction (EBSD) measurement. The specimens for the EBSD examination were prepared by mechanical grinding and final polishing with a colloidal silica slurry. The accelerating voltage of 20 kV, a tilt angle of 70°, and a step size of 0.1 μm were applied to study the orientation relationships between the microstructure's constituents, and the variant selection mechanism of bainitic ferrite plates. Microstructural characterization in the nanoscale was performed using a Tecnai FEG G2 F20 Super Twin transmission electron microscopy (TEM) at 200 kV. Thin foils to TEM observations were electro-polished using a Tenupol-5 jet-polisher in an electrolyte consisting of 10 vol.% of HClO_4 in methanol at -25 °C. The true thickness

of bainitic ferrite plates was measured using the mean linear intercept method [38]. To further confirm the presence and the volume fraction of identification phases and global texture, X-ray synchrotron radiation ($\lambda = 0.0142342$ nm) was used [39, 40]. The Rietveld refinement was performed to determine lattice parameters and volume fraction of ferrite (α -Fe) and austenite (γ -Fe) using High Score Plus. The carbon concentration of retained austenite (C_γ) was calculated using Eq. 2 [28]:

$$C_\gamma \approx \frac{a_\gamma - 3.5780}{0.033} \quad (2)$$

where a_γ is the austenite lattice parameter in Å. In addition, using the X-ray synchrotron diffraction pattern, the dislocation density (ρ) in α -Fe and γ -Fe was calculated using Eq. 3 [41]:

$$\rho = \frac{2\sqrt{3}\epsilon^{2/2}}{Db} \quad (3)$$

where $\langle \epsilon^2 \rangle^{1/2}$ is the lattice microstrain (depending on measured broadening and 2θ position of peaks determined based on Williamson–Hall plot), b is a Burgers vector (for body-centered cubic (BCC) metals, b along $\langle 111 \rangle$ is $\frac{\sqrt{2}}{2}a_\alpha$, for face-centered cubic (FCC) metals, b along $\langle 110 \rangle$ is $\frac{\sqrt{3}}{3}a_\gamma$) of dislocations in nm and D is a crystallite size for austenite and ferrite also determined based on Williamson–Hall plot. Diffraction experiments were performed in transmission geometry in order to ensure good statistics, while the microstructure investigations were done on the traverse cross-section to the rolling direction (TD). Mechanical properties were selected based on the uniaxial tensile tests using an MDS 830 Bähr Thermoanalyse testing machine at the strain rate of 1 s^{-1} . This testing machine was also used to determine the kinetics of bainitic transformation by applying torsion deformation during isothermal holding at 200°C for 10 s after austenitization at 950°C for 5 min and before holding at 200°C for 10 min and yield strength of parent austenite. Tests were carried out under nitrogen protect atmosphere, and changes in length and radius were measured by the laser measurement system. Furthermore, using a Bähr 805A high-resolution dilatometer, the kinetics of bainitic transformation and critical temperatures (without applying external stress) were determined. An induction heating coil supported the heating and cooling of specimens with 4 mm in diameter and 10 mm in length. The tests were also carried out under nitrogen protect atmosphere, and quartz push-rods in direct contact with the sample measured the longitudinal changes in length. The temperature was controlled using thermocouple type S in both dilatometric tests with and without additional external stress during bainitic transformation. In addition, the Vickers hardness tests were

carried out using a Zwick/ZHU 250 (HV5) machine with a load of 49 N for 15 s. The impact tests were conducted at room temperature with a Zwick/Roell RKP 450 testing machine on samples with a dimension of $10 \times 10 \times 55$ mm with U-shaped notches.

3 Results and discussion

3.1 Determining bainitic transformation's kinetic

To determine the bainitic transformation's kinetic of tested steel, dilatometric measurements and torsion deformation in the range of isothermal holding were carried out. During the thermal simulation, samples were heated up to 950°C with 5°C/s to austenitization temperature, held for 5 min, and rapidly cooled down to 200°C , i.e., bainitic reaction temperature. After reaching the isothermal temperature, the samples were held for 30 s and subsequently subjected to torsion deformation using stress below the yield strength of parent austenite (250 MPa). After that, the samples were held for 10 min to analyze the behavior of bainitic transformation kinetics. Figure 2a shows the thermal dilatation curve indicating a negative relative change in length (RCL) in the longitudinal direction (black curve) and a positive relative change in radius (RCR) in the radial direction (red curve). The negative effect of RCL, which has been chiefly reported when nanobainitic transformation occurs under external stress, particularly below the yield stress of austenite, may be explained by variant selection giving rise to anisotropic transformation [37]. In addition, Ref. [42] indicates that the RCR should not be used to determine the bainitic transformation kinetic under stress and emphasize that the best way to analyze the kinetic of bainitic transformation under stress is a relative volume change (RCV). Hence, Fig. 2b shows the RCV determined based on reference [43] in the function of bainitic transformation time. In addition, according to the following literature [44], one of the methods to determine the end of bainitic transformation proposed by Santajuana et al. was applied. It is the 4% of the maximum value of the normalized first derivative of the relative change volume (Normalized RCV). Figure 3 shows the Normalized RCV in the function of isothermal holding time during bainitic transformation. Analyzing this result, it is clear that the end of bainitic transformation in the case of tested steel is less than 10 min. These results indicated that the bainitic transformation significantly accelerates after applying the torsion stress for 10 s.

In addition, the critical transformation temperatures from dilatometric heating and cooling tests were measured. In the case of steel subjected to bainitic transformation with external stress below the yield stress of parent austenite, the A_{C1} , A_{C3} , and martensitic start (M_s) temperatures without

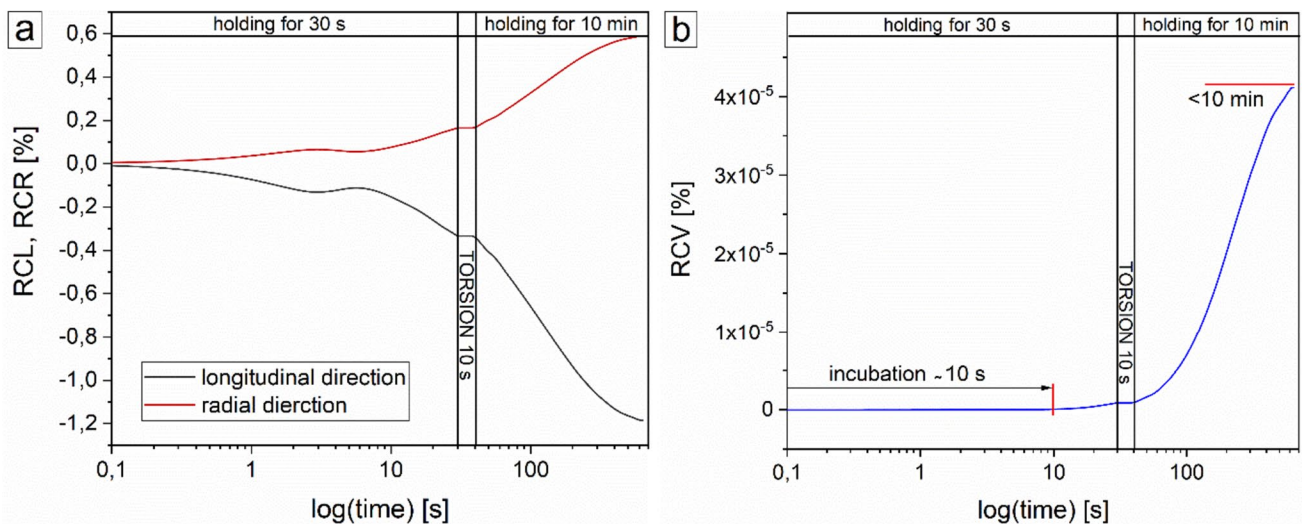
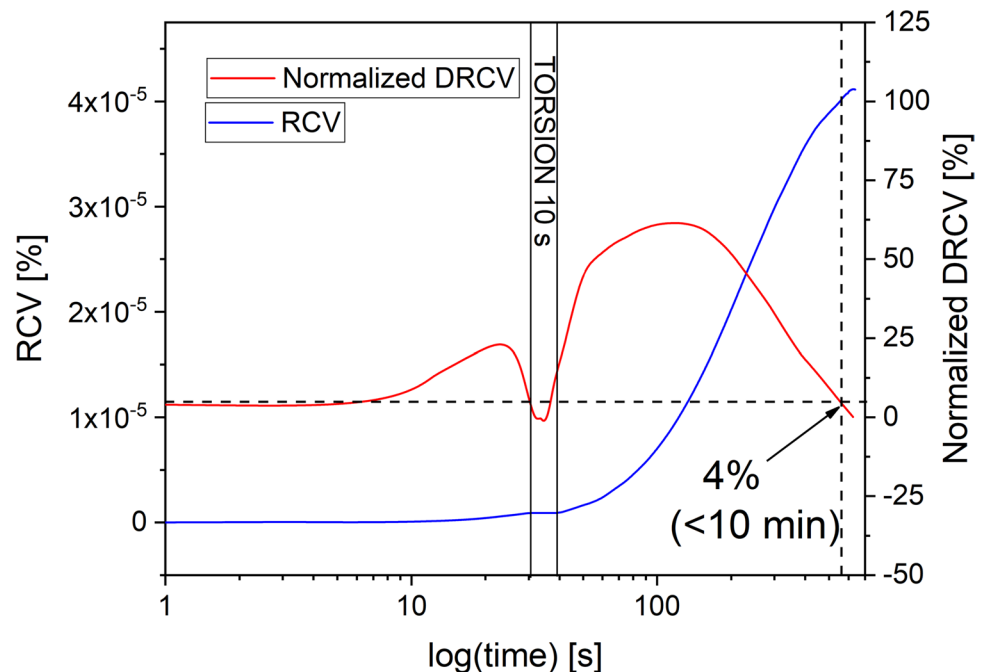


Fig. 2 The dilatometric curves showing the nanobainitic transformation kinetic's at 200 °C with applied torsion strain of experimental steel: **a** in the radial (red curve) and in the longitudinal (black curve) direction, **b** in the volume (blue curve) of the specimen

Fig. 3 The relative volume change (RCV), together with the normalized first derivative of relative volume change (Normalized DRCV) of the sample obtained during dilatation experiments with additional external stress



and after this treatment were determined at 730 °C, 850 °C, 122 °C, and 31 °C, respectively.

Moreover, using the equation given in Ref. [45], the bainitic start (B_s) temperature was calculated as 316 °C. Determining initial M_s and B_s temperatures are essential because these temperatures define the range of the nanobainitic transformation. In our case, the temperature interval in which nanobainitic transformation takes place falls within the range between 122 °C and 316 °C. Moreover, knowing that the additional external stress can increase the bainitic transformation temperature up to 60 °C applying the stress on the

200 MPa in the case of high-carbon nanobainitic steel [23], and for economic reasons, the bainitic transformation of the reference steel was carried out at 280 °C for 3 days. The isothermal holding at 200 °C for 3 days was also carried out; however, the bainitic transformation was not completed. In addition, the obtained austenite was not stabilized ($M_s > RT$). The martensite start temperature of the tested steel, obtained by conventional heat treatment, was determined based on dilatometric measurements. During dilatometric tests, the steel was subjected to austempering treatment consisting of austenitization at 950 °C for 5 min, rapid cooling to 280 °C,

holding for 3 days, and fast cooling to room temperature. Based on these results, the M_s temperature was determined as below 25 °C, and 3 days is long enough to partition the carbon between the microstructure's constituents and obtain high-carbon nanobainitic steel at 280 °C. The chemical composition and described thermal simulations can allow obtaining the nanostructured bainitic steel with the microstructure consisting of the bainitic ferrite laths and retained austenite in the time of bainitic transformation of about 10 min. In contrast, without applying additional stress in the range of isothermal holding at 280 °C, the same steel needs 3 days to complete the nanobainitic transformation. Comparing these results, it is clear that applying the novel thermomechanical treatment causes the incredible acceleration of bainitic transformation kinetic even at ultra-low transformation temperatures.

3.2 Microstructure and phase compositions

The LOM and SEM micrographs of the experimental high-carbon nanobainitic steel subjected to the controlled thermomechanical treatment are shown in Fig. 4. The optical image in Fig. 4a shows a typical microstructure consisting of bainitic sheaves (darker phase, exemplary marked as bainite sheaf) randomly oriented to each other and blocky retained austenite (bright phase, marked as γ_b) with an average size of $1.17 \pm 0.31 \mu\text{m}$ measured based on SEM-BSE micrographs. Figure 4b shows the SEM-BSE micrograph, with the microstructure containing the bainitic ferrite (darker phase, marked as α_{BF}) and retained austenite with different morphology in the shape of the thin films (brighter phase, marked as γ_f).

Figure 5a shows the high-resolution X-ray synchrotron diffraction pattern taken from the same sample, which confirms two phases, α -Fe and γ -Fe. The volume fraction of ferrite (V_α) and austenite (V_γ), as well as their lattice parameters, were found to be $56.9 \pm 2.0\%$, $2.8728 \pm 0.0002 \text{ \AA}$ (a_α) and $43.1 \pm 1.2\%$, $3.6166 \pm 0.0001 \text{ \AA}$, respectively. The carbon concentration in the austenite (C_γ) was determined as $1.17 \pm 0.09 \text{ wt.}\%$, using Eq. 1, and dislocation density in bainitic ferrite (ρ_α) and retained austenite (ρ_γ) have also been calculated using Eq. 2. The peak of (200) Fe- γ is one of the most appropriate for the identification of high-carbon (RA in the shape of film-like), and low-carbon (RA in the form of blocky) retained austenite [46]. The enlargement of the (200) Fe- γ peak is shown in Fig. 5b. The asymmetric peak is deconvoluted using the Gaussian multi-peaks fitting method [47]. Peak separation of the (200) Fe- γ into two independent peaks provides two areas: the first corresponds to the film-like high-carbon retained austenite (γ_f , red curve in Fig. 5b) with a carbon concentration of $1.93 \pm 0.14 \text{ wt.}\%$ (C_{γ_f}), while the second to the blocky retained austenite (γ_b , blue curve in Fig. 5b) with a carbon concentration of $1.18 \pm 0.09 \text{ wt.}\%$ (C_{γ_b}). In addition, the volume fraction of film-like and blocky retained austenite was also determined. The obtained parameters for both phases are summarized in Table 1.

One of the most critical factors in the mechanical stability of retained austenite is its chemical composition and morphology. Films of retained austenite consist of a higher carbon concentration (the high level of mechanical stability) and are more stable than blocky. Therefore, they do not transform into martensite during plastic deformation.

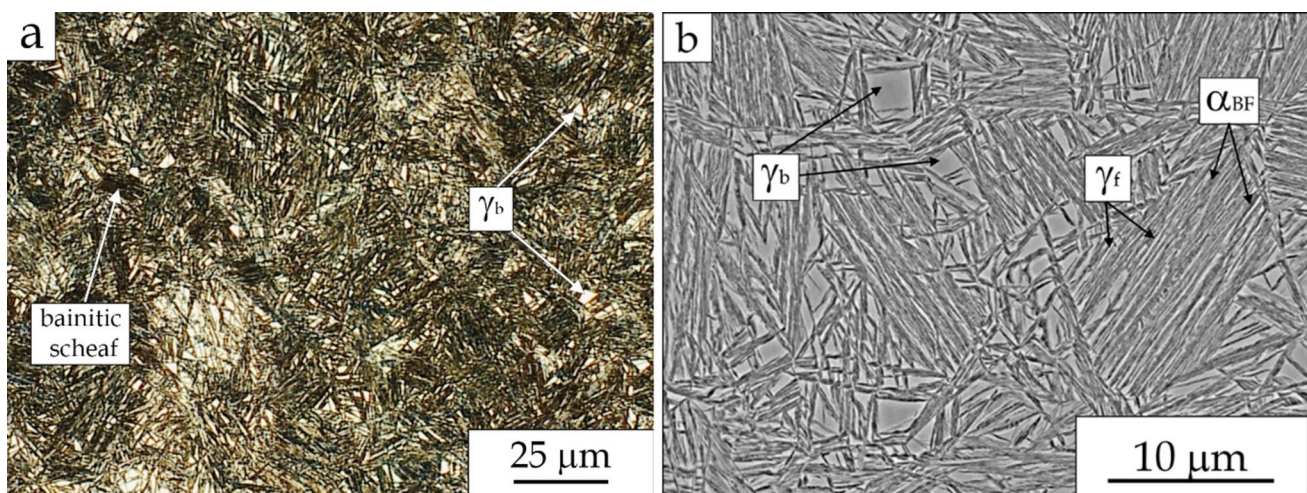


Fig. 4 Optical microstructure **a** and SEM-BSE micrograph **b** of high-carbon nanobainitic steel obtained by the controlled thermomechanical treatment

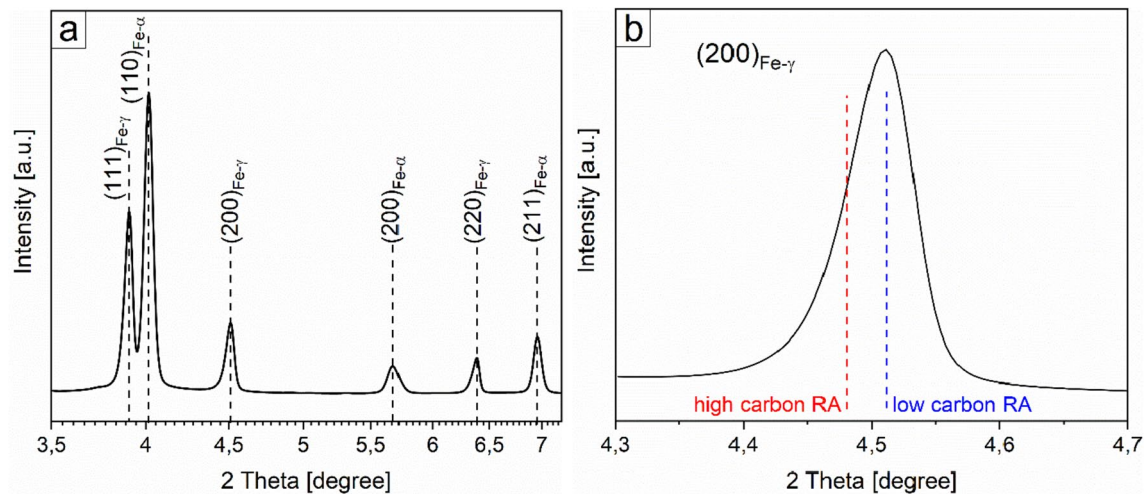


Fig. 5 The XRD diffraction pattern of the presented high-carbon nanobainitic steel (a), and the deconvolution of (200)Fe- γ peak (b). Red curve and blue curve refer to high-carbon and low-carbon retained austenite, respectively

Table 1 Characteristic of bainite microstructure of high-carbon nanobainitic steel

Bainitic ferrite				Retained austenite			
V_{α} [vol%]	a_{α} [Å]	ρ_{α} [10^{15} m^{-2}]	$t_{\alpha_{BF}}$ [nm]	V_{γ} [vol%]	a_{γ} [Å]	ρ_{γ} [10^{14} m^{-2}]	C_{γ} [wt.%]
56.9 ± 2.0	2.8728 ± 0.0002	1.85	68 ± 40	43.1 ± 1.2	3.6166 ± 0.0001	1.07	1.17 ± 0.09
Film-like retained austenite (γ_f)				Blocky retained austenite (γ_b)			
V_{γ_f} [vol%]	a_{γ_f} [Å]	C_{γ_f} [wt.%]	t_{γ_f} [nm]	V_{γ_b} [vol%]	a_{γ_b} [Å]	C_{γ_b} [wt.%]	t_{γ_b} [μm]
14.5 ± 1.0	3.6416 ± 0.0003	1.93 ± 0.14	34 ± 17	35.0 ± 1.5	3.6169 ± 0.0003	1.18 ± 0.09	1.17 ± 0.31

On the other hand, according to the literature [48, 49], when the carbon concentration in austenite is higher than 1.0 wt.%, it is too stable to transform into martensite. In such a case, the TRIP effect may be bypassed.

3.3 Crystallographic orientation relationships and texture examination

To confirm the presence of the given phases and to determine the crystallographic orientations between them, the SEM/EBSD technique was applied. Figure 6a and b shows the phase distribution map and inverse pole figure (IPF) map for identified phases, respectively. Based on Fig. 6a, we can distinguish only two phases, i.e., the retained austenite represented by green color, and the bainitic ferrite represented by red color. In the IPF color map of bainitic ferrite and retained austenite, colors correspond to transverse direction according to the stereographic triangle.

Figure 7 shows an IPF map of a cubic oriented grain of the parent austenite represented by {001}, and {111} pole figures (PFs) and {001}, and {101} PFs of bainitic ferrite. The analysis of both PFs confirms Nishiyama–Wasserman shows orientation relationships in this grain [50, 51]. This orientation relationship can be easily recognized by 4 different orientations located symmetrically concerning each of the three main axes of austenite in Fig. 7. For instance, 4 orientations in the middle of the {001} PF direction can be found (red variants rotated a few degrees towards $\langle 110 \rangle$). In addition, the PFs of bainitic ferrite allow us to notice that the cubic oriented grain of parent austenite shows three different groups of orientations of bainitic ferrite plates after controlled thermomechanical treatment (austenite orientation indicated by black poles). The orientation relationship was also studied with higher statistics using the whole EBSD map by misorientation distribution function (MDF) shown in Fig. 8. These results clearly indicate three different relationships between austenite and

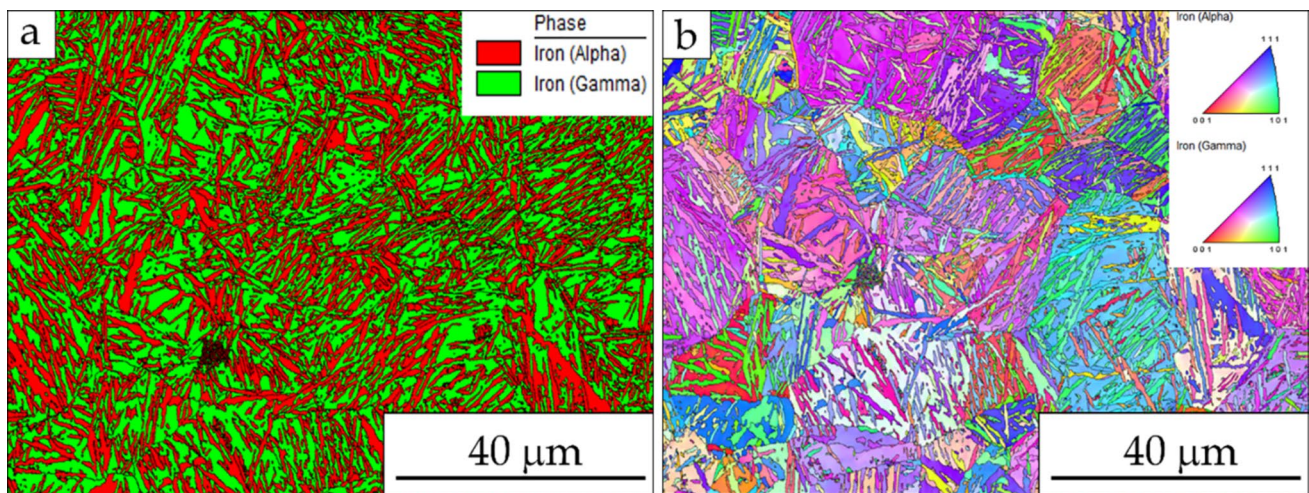


Fig. 6 SEM/EBSD microstructure of presented high-carbon nanobainitic steel: **a** distribution map and **b** inverse pole figure (IPF) map orientation of identified phases

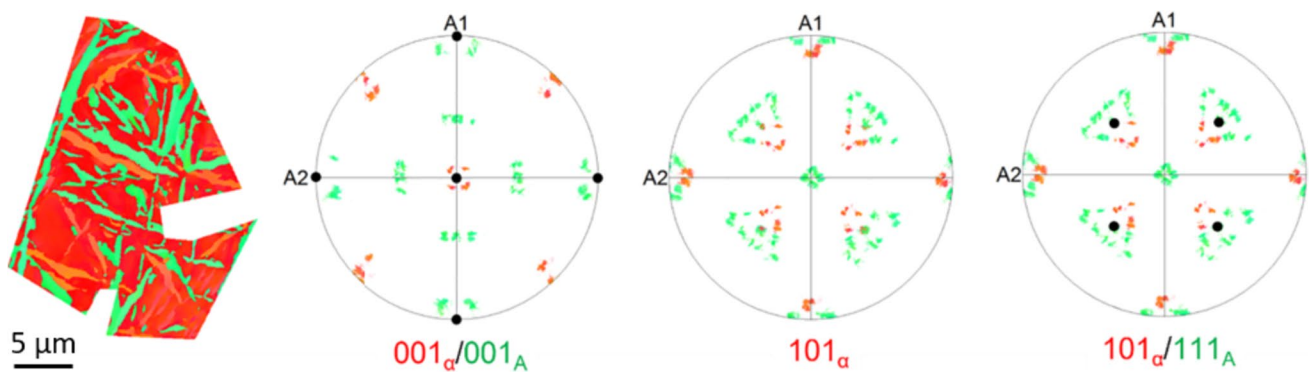


Fig. 7 Inverse pole figure (IPF) map of a cubic austenite grain and corresponding superposition of $\{001\}_\alpha$ and $\{001\}_A$, as well as $\{101\}_\alpha$ and $\{111\}_A$ pole figures of bainitic ferrite and austenite presenting

the N–W orientation relationship. Austenite orientation is represented by black poles, while red and green correspond to different bainitic variants

bainitic ferrite: with much stronger N–W than two other relations K–S and Pitsch relation. In contrast, Beladi and his co-workers [2, 52] highlight that in the non-ausformed nanobainitic steel obtained at 200 °C for 10 days with a similar chemical composition, the crystallographic orientation relationships between bainitic ferrite and austenite is closer to K–S than N–W. Therefore, a few authors indicated that applying the ausforming process results rather in obtaining the nanobainitic steel close to N–W than K–S crystallographic ORs between bainitic ferrite laths and austenite [30, 48]. For illustration, Fig. 8b presents the phase distribution map with select crystal orientation relationships. The boundaries between bainite and austenite are colored red, navy blue, and green for N–W, K–S, and Pitsch relations, respectively. The other PFs given in Fig. 6 show the typical relation between the most closed-packed plane of BCC and FCC lattice with the parallelism of $\{110\}_\alpha$ and $\{111\}_A$.

This analysis concludes that applying the stress-induced nanobainitic transformation prefers the N–W crystallographic orientations of bainitic variants in the range of not only one austenite grain but also from the global perspective [2, 52]. In addition, specific crystallographic orientation variants of the bainitic ferrite phase on the presented pole figures are slightly blurred, which indicates some rotation and is associated with that shear deformation during applying deformation in the elastic strain range. According to some references [37, 43, 53], the very low temperature of bainitic transformation and stress-induced or strain-induced bainitic transformation are the reasons for bainitic ferrite variant selection during bainitic transformation and built the anisotropic microstructure. These considerations were confirmed by dilatometric measurements presented in the discussed section.

Figure 9 shows the (111), (200), and (220) synchrotron XRD pole figures of bainitic ferrite and retained austenite

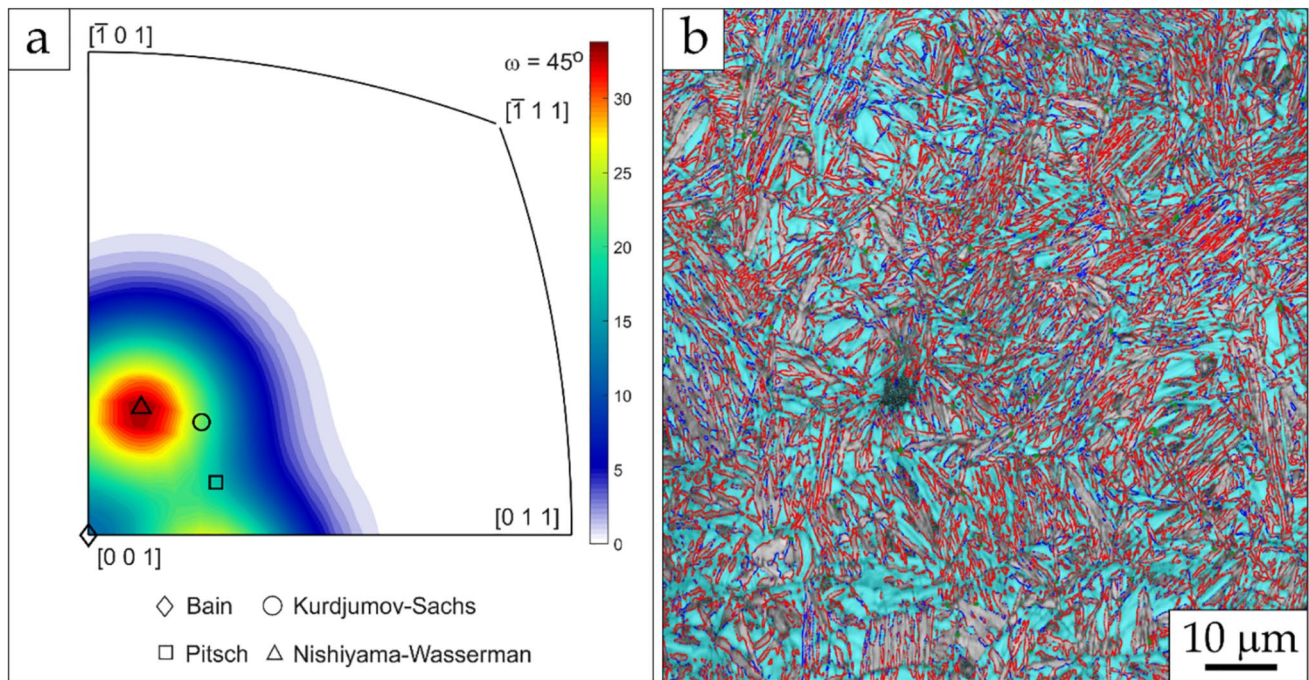


Fig. 8 **a** MDF for retained austenite/bainitic ferrite with the key relations: Nishiyama–Wasserman (triangle), Kurdjumov–Sachs (circle), Pitsch (square), and Bain (diamond). **b** Phase distribution map

(ferrite-grey, austenite-blue) with the indicated N–W misorientation angles in red, K–S misorientation angles in navy blue, and Pitsch misorientation angle in green

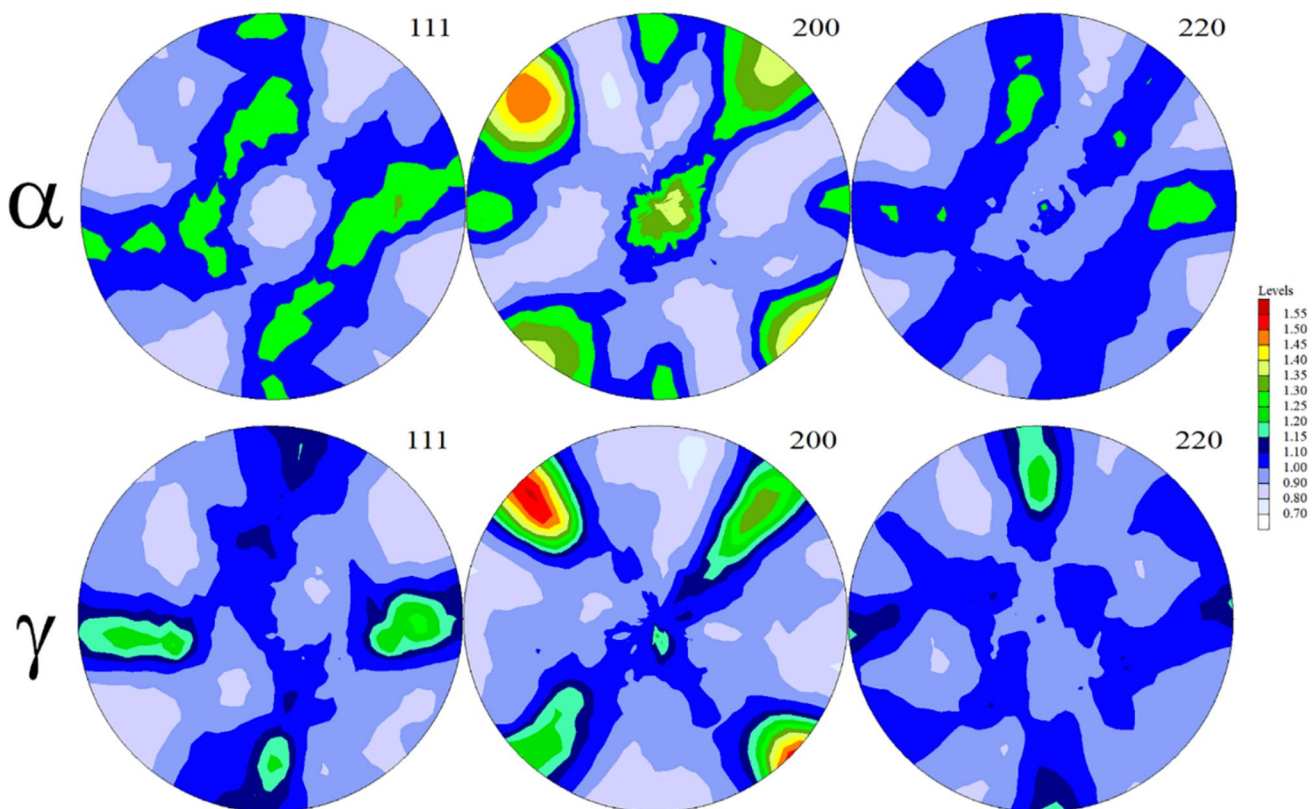


Fig. 9 (111), (200), and (220) pole figures of bainitic microstructure components of the high-carbon nanobainitic steel

of high-carbon nanobainitic steel after the controlled thermomechanical treatment. The crystallographic texture of retained austenite consists mainly of the shear component of $(110) \langle 100 \rangle$. In contrast, the bainitic ferrite consists of the dominant shear component of $(110) \langle 100 \rangle$ and, less visible, the cubic component of $(100) \langle 001 \rangle$. As previously mentioned, the application of stress during bainitic transformation causes an increase in the total driving force by introducing an additional mechanical driving force (shear components) which promotes the growth of specific variants of bainitic ferrite. In work [31], the authors applied the continuous external tensile stress of 0 MPa, 50 MPa, and 100 MPa (stress below the yield strength of parent austenite) during bainitic transformation in order to obtain lower bainite. In the case of this microstructure, they indicated that more favored variants of bainitic ferrite laths are created during isothermal heat treatments, with $[101]$ - and $[201]$ -orientations parallel to

the tension axis. In another work [54], the same authors analyzed the influence of external stress, also below the yield stress of parent austenite in terms of tensile stress. In this case, they reduced the external stress to 0 MPa before the bainitic transformation was completed (50% of the maximum TP strain). These results, which were also obtained in the range of lower bainite, indicate the favored variants growth of bainitic ferrite laths. However, the external stress is not large enough to continue the growth of these variants after removing the stress. By comparing these considerations to the results shown in Fig. 9, we can recognize the shear component of $(110) \langle 100 \rangle$ with high intensity and the less pronounced cubic component of $(001) \langle 001 \rangle$ of bainitic ferrite plates. This observation indicates that the additional loading applied to the samples after 30 s created the main shear component of bainitic variants. After removing loading, the external stress was enough to cause the large TP strain in the structure

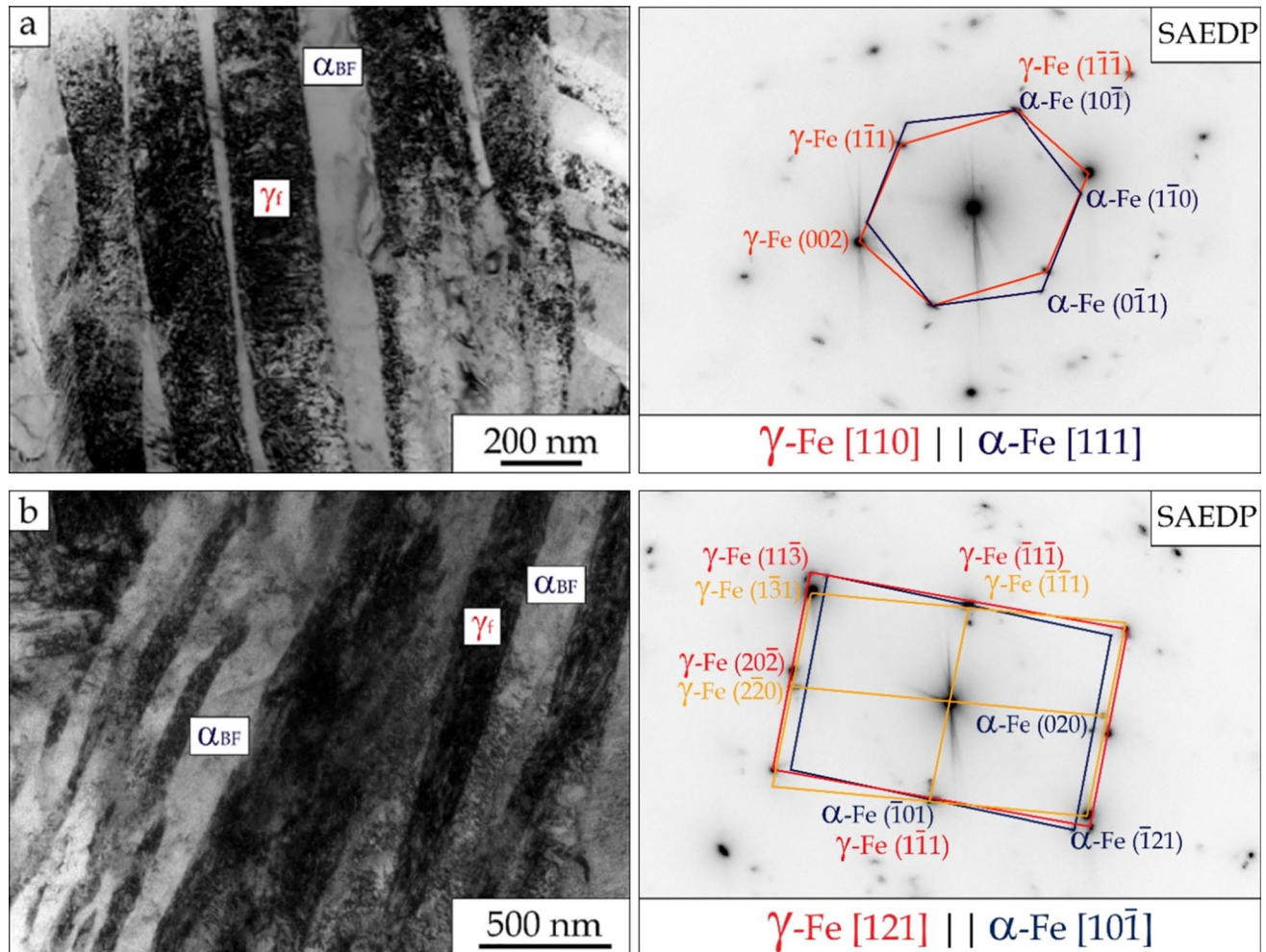


Fig. 10 TEM-BF images and corresponding SAEDPs of presented high-carbon nanobainitic steel showing: **a** K-S and **b** N-W orientation relationships between austenite and bainitic ferrite plates

and allow for growing the favored variants during further nanobainitic transformation.

The TEM observations were employed to resolve fine details of the microstructure, especially in the case of nanobainitic structure. Figure 10 presents a set of the bright-field TEM micrographs (TEM-BF) and corresponding selected-area electron diffraction (SAED) patterns. The TEM-BF images in Fig. 10a and b confirm that the films of retained austenite with an average size of 34 ± 17 nm are parallel to plates of bainitic ferrite with an average size of 68 ± 40 nm in all observed volumes of the sample. The SAED pattern obtained from the whole area of the sample presented in the bright-field image in Fig. 10a reveals strong reflections coming from $(1\bar{1}1)$ and (002) in the Fe- γ with $[110]$ zone axis, whereas weak reflections are from $(0\bar{1}1)$ and $(1\bar{1}0)$ planes from the Fe- α with $[111]$ zone axis. Another Fe- γ and Fe- α substructure was discovered based on SAED patterns obtained from the microstructure shown in Fig. 10b. In this case, strong reflections from $(20\bar{2})$ and $(11\bar{3})$ planes of Fe- γ with $[121]$ zone axis and weak reflections from $(\bar{1}21)$ and (020) planes of the Fe- α with $[10\bar{1}]$ zone axis were indicated. In addition, the SAED pattern shown in Fig. 10b, presents other substructure of Fe- γ (labeled with yellow color) with $[121]$ zone axis. The cementite precipitation on bainitic ferrite/retained austenite boundaries was not detected because the level of applied silicon content in the high-carbon nanobainitic steel is above 1.5 wt.% [55]. In addition, the aluminum content, together with applied external stress during bainitic transformation, led to obtaining the carbide-free bainitic steel [23, 26]. It is generally known that in the high-carbon nanobainitic steel, the orientation relationships (ORs) between austenite and bainitic ferrite change from Nishiyama–Wassermann $((111)_{\gamma} \parallel (011)_{\alpha}, [11\bar{2}]_{\gamma} \parallel [01\bar{1}]_{\alpha})$ to Kurdjumov–Sachs (K–S, $(111)_{\gamma} \parallel (011)_{\alpha}, [10\bar{1}]_{\gamma} \parallel [11\bar{1}]_{\alpha})$ depending upon the ratio of lattice parameters [56]. Based on the SAED patterns presented in Fig. 10, it can be stated that the orientation relationships between films of retained austenite and plates of bainitic ferrite correspond very well either to Kurdjumov–Sachs $((111)_{\gamma-Fe} \parallel (10\bar{1})_{\alpha-Fe}, [110]_{\gamma-Fe} \parallel [111]_{\alpha-Fe})$ or Nishiyama–Wassermann $((111)_{\gamma-Fe} \parallel (\bar{1}01)_{\alpha-Fe}, [121]_{\gamma-Fe} \parallel [10\bar{1}]_{\alpha-Fe})$ relations, what also was observed in Ref. [52].

3.4 Mechanical properties

The tensile tests and Vickers hardness tests were conducted to determine the mechanical properties of the presented

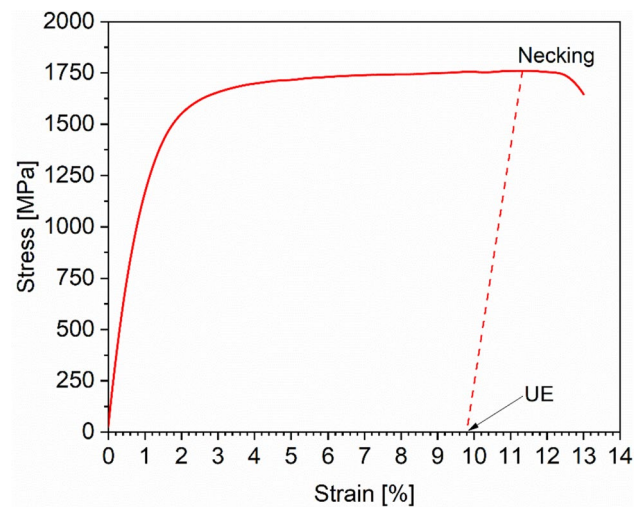


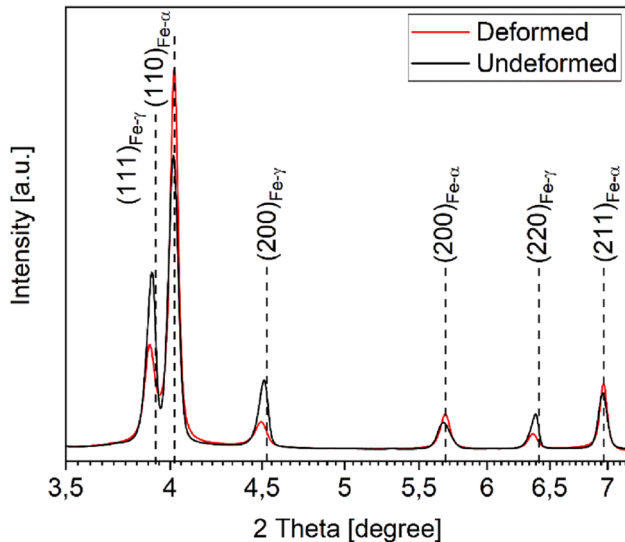
Fig. 11 The stress–strain curve of high-carbon nanobainitic steel fabricated by controlled thermomechanical treatment

high-carbon nanobainitic steel. Figure 11 shows the representative stress–strain curve, and Table 2 summarizes the obtained results. The novel thermomechanical treatment application leads to obtaining an ultra-high strength and ductility steel after an incredibly short time of isothermal holding (30 min). Due to well-known factors, the high-carbon nanobainitic steel achieved the ultimate tensile strength of approximately 1862 ± 140 MPa and yield strength of approximately 1287 ± 90 MPa. The strength properties mainly depend on the mean thickness of the bainitic ferrite plates and the dislocation density [55]. In addition, increasing the Al content from 0.5 wt.% to nearly 1.5 wt.% can improve the tensile strength and enhance elongation [57]. The high elongation at $11.8 \pm 0.7\%$ was obtained first due to the high amount of retained austenite in steel [49]. In comparison, the uniform elongation of described steel is slightly lower ($9.8 \pm 0.8\%$) than the total elongation. In addition, the impact toughness of tested steel is 88 ± 7 J/cm² and is higher than that of the steels obtained by conventional heat treatment and compiled in an article [6]. These results indicated excellent mechanical behavior.

Further improvement in mechanical properties enables the transformation-induced plasticity effect (TRIP effect) [58]. As well known, the TRIP effect relies on transforming retained austenite into martensite during a tensile test because of large deformation. The mechanical stability of austenite mainly depends on the carbon concentration in the retained austenite and its morphology [49]. Olson and Cohen [59] indicated that the M_s temperature slightly increases with the first stage of applied deformation (in the range of elastic deformation). As commonly known, the blocky retained austenite has a lower carbon concentration than thin films of

Table 2 The summarized mechanical properties of high-carbon nanobainitic steel

UTS [MPa]	YS [MPa]	TE [%]	UE [%]	Hardness [HV5]	Impact toughness [J/cm ²]
1862 ± 140	1287 ± 90	11.8 ± 0.7	9.8 ± 0.8	586 ± 16	88 ± 7

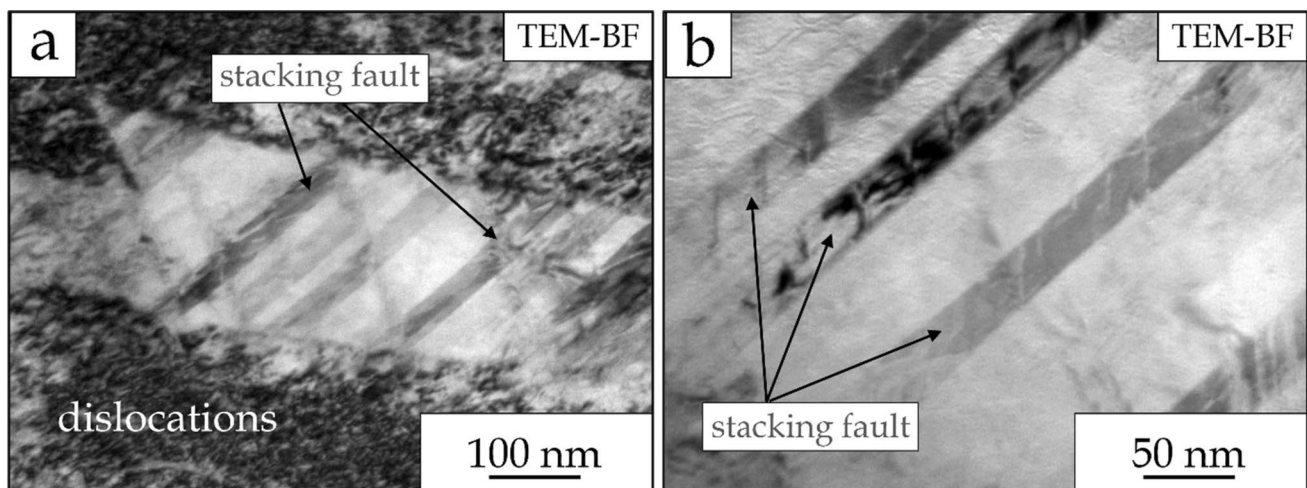
**Fig. 12** The XRD synchrotron pattern of high-carbon nanobainitic steel after tensile deformation

retained austenite. Hence, the blocky retained austenite can be favored for martensite transformation during the tensile test.

The first evidence for the TRIP effect during tensile deformation took place and its increasing of the total hardness in the distance a few millimeters from the place of the

fracture surface of the specimen after the tensile test, which is approximately 662 ± 37 HV5. In addition, Fig. 12 compares the XRD synchrotron diffraction patterns of the high-carbon nanobainitic steel before (marked as a black line) and after (marked as a red line) tensile deformation. Based on these results, the basic parameters were determined. The volume fraction of retained austenite in the sample after the tensile test decreased from 43.1 ± 1.2 to 28.2 ± 1.5 vol%, with a higher lattice parameter of 3.6305 ± 0.0001 Å and a higher carbon concentration of 1.59 ± 0.12 wt.%. In addition, peaks of martensite, which are created during tensile deformation, and ferrite have the same 2θ positions, and the peaks of martensite are shifting and broadening toward ferrite. The same changes of mentioned parameters in the nanobainitic steel after deformation, which confirmed that the TRIP effect occurred, are described in Ref. [3]. These results demonstrate that the TRIP effect took place during tensile deformation and increases the total elongation of experimental steel through the transformation of blocky retained austenite into martensite because this morphology of retained austenite requires lower driving force for martensite nucleation. In addition, the blocky morphology of retained austenite has a smaller carbon concentration and can transform into martensite, especially in the first stage of deformation strain [60].

Apart from the TRIP effect, the twinning-induced plasticity (TWIP) effect can increase the yield strength

**Fig. 13** a High- and b low-magnification TEM-BF micrographs with the stacking faults (mechanical twins) in the film of retained austenite of experimental steel after tensile deformation

of steel [61, 62]. This effect was also observed in the presented experiment. Figure 13a and b shows the TEM images observed in the bright field. The detailed TEM observation of the specimen after tensile deformation reveals that the stacking fault exists in the retained austenite, which can be created by partial dislocation movement across the austenite grain on the (111) slip plane [63]. The mechanical twinning can occur in the film-like retained austenite due to higher mechanical stability than blocky retained austenite [64]. In addition, Poddar and his co-workers [65] emphasize that stacking fault in the microstructure is attributed to lower stacking fault energy (SFE) of retained austenite, which confirms that twins are formed during tensile straining and improve ductility. In this work, the authors suppose that stacking fault (mechanical twins) with an average size of 29 ± 5 nm growth in film-like retained austenite when the SFE is large enough. In addition, the boundaries of twins can interact with dislocations and influence strain hardening deformation due to structure refinement [66]. Moreover, dislocations are observed near mechanical twins formed in the film of retained austenite. According to Ref. [67], the kind of deformation mechanisms (twinning or dislocation glide) in the face-centered cubic metals is strongly connected with their stacking fault energy value. In his case, twinning and simultaneously TWIP occur when SFE is located in the range between 18 mJ m^{-2} and 45 mJ m^{-2} . In addition, in this case, mainly the chemical composition of austenite influences the SFE value. This value increases especially by Mn and Al (the dissolved elements) content in the austenite. The authors, using mathematical considerations on the example of TWIP steels presented in Refs. [67, 68], estimate the ideal stacking fault energy for described steel with raised content of C, Mn, and Al is 23 mJ m^{-2} . Based on this, from a theoretical point of view, mechanical twinning during tensile deformation is possible. However, more evidence, like detailed TEM observations, is necessary to confirm this theory because there are no reports on this effect in the case of carbide-free bainitic steel obtained by thermomechanical treatment.

In order to compare the mechanical properties of presented high-carbon nanobainitic steel manufactured by the controlled thermomechanical treatment to the steel obtained by conventional heat treatment, we refer to Ref. [69], where the authors obtained high-carbon nanostructured bainitic steel by isothermal holding at 200°C for 3 days without additional external stress in the range of bainitic transformation with the similar chemical compositions to presented experimental steel. In this case, the steel also contains cobalt (Co) at 1.37 wt.%, and as well

known, this alloying element reduces the total time of bainitic transformation [18]. The mentioned high-carbon nanobainitic steel has achieved the UTS of approximately 2.2 GPa, YS of approximately 1.4 GPa, and total elongation at 8%. However, despite the higher strength properties, it is noted that the total time of nanobainitic transformation was reduced to 30 min, and the total elongation is higher in the case of steel obtained by thermomechanical treatment because during tensile deformation, probably the TWIP effect was noticed in contrast to steel obtained by conventional heat treatment. We can also find other examples of steels obtained by conventional heat treatment with isothermal transformation at 200°C for 3 days with chemical compositions similar to the presented experimental steel [70] and steel shown in Ref. [59]. In the case of nanostructured bainitic steel, the authors obtained high-strength properties with UTS below 2.0 GPa and YS below 1.9 GPa, but the total elongation of this steel is around 1%. This steel needs 3 days to obtain the nanobainitic microstructure, and plastic properties are inferior compared to the presented experimental steel obtained by controlled thermomechanical treatment. In the case of tested steel isothermally treated at 280°C for 3 days without external stress during bainitic transformation (reference steel), the basic strength properties were determined in the uniaxial tensile tests. Compared to the steel manufactured by controlled thermomechanical treatment, ultimate tensile strength, yield strength, and elongation of the steel obtained by the conventional heat treatment are lower and are $1386 \pm 16 \text{ MPa}$, $989 \pm 4 \text{ MPa}$, and $4.5 \pm 0.4\%$, respectively. Applying the described thermomechanical treatment enhances the UTS, YS, and A by about 476 MPa, 298 MPa, and 7.3%, respectively. To summarize, this has to be emphasized that the bainitic transformation time of tested steel allows obtaining the nanobainitic microstructure was reduced from 3 days to 30 min, and simultaneously the mechanical properties were improved.

Figure 14 shows the SEM microstructures of the fracture surface in the places marked as regions 1 and 2. The fracture of the tensile sample consists of the cup and cone, which do not exist in the area of the external surface of the specimen at the region marked as 2. In the region marked as 1, the depth dimples formed by microvoid coalescence, high density of undulating facets, and tearing edges were observed. These factors reveal the ductile behavior of features [71]. In addition, the limited quasi-cleavage facets have not been observed in region 2, which can partly weaken the plasticity of high-carbon nanobainitic steel. The high resistance of cleavage fracture is probably due to the absence of carbide precipitation [72].

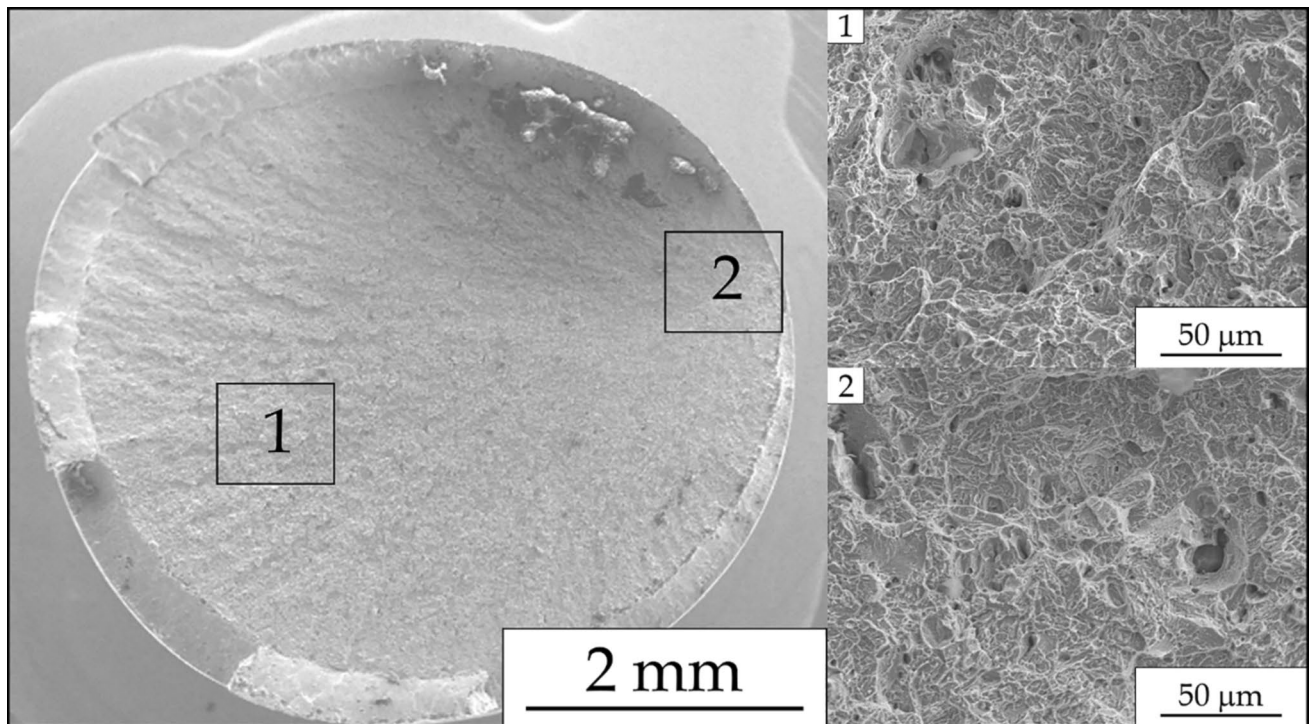


Fig. 14 SEM fractography of the specimen obtained through controlled thermomechanical treatment after tensile test

4 Conclusions

- Applying the controlled thermomechanical treatment consisting of austenitization at 950 °C/5 min, followed by applying the external stress on the level of 250 MPa at 200 °C and then holding at 190 °C for 30 min led to the formation of the nanobainitic microstructure comprising bainitic ferrite laths with an average size of 68 ± 40 nm and retained austenite in the shape of films with an average size of 34 ± 17 nm. In addition, blocky retained austenite with an average size of 1.17 ± 0.31 μm was identified.
- TEM observations indicated the K–S and N–W crystallographic orientation relationships between the ferritic and austenitic phases, while SEM/EBSD and MDF techniques confirmed that the application of controlled thermomechanical treatment produced mainly N–W OR in this high-carbon nanobainitic steel.
- The crystallographic texture analysis suggests that the main bainitic ferrite growth occurs during isothermal holding after removing the external stress in the form of torsion stress. A $(110) \langle 100 \rangle$ shear component of bainitic ferrite can indicate that this stress applied in the elastic strain range accelerates the growth of favored crystallographic orientation and thereby accelerates the nanobainitic transformation.

- The high ultimate tensile strength of 1862 ± 140 MPa and yield strength of 1287 ± 90 MPa were achieved, most probably due to the nano-metric size of bainitic ferrite and its high dislocation density. The TRIP and TWIP effects were noticed in the samples after tensile tests. These effects give rise to a high level of elongation at $11.8 \pm 0.7\%$.

Acknowledgements This research was supported by The National Research and Development Centre, Poland (Project No POIR.01.01.01-00-0418/19-00).

Data availability Data will be made available on request.

Declarations

Conflict of interest On behalf of all the authors, the corresponding author states that there is no conflict of interest.

Ethical standards Informed consent.

Open Access This article is licensed under a Creative Commons Attribution 4.0 International License, which permits use, sharing, adaptation, distribution and reproduction in any medium or format, as long as you give appropriate credit to the original author(s) and the source, provide a link to the Creative Commons licence, and indicate if changes were made. The images or other third party material in this article are included in the article's Creative Commons licence, unless indicated otherwise in a credit line to the material. If material is not included in

the article's Creative Commons licence and your intended use is not permitted by statutory regulation or exceeds the permitted use, you will need to obtain permission directly from the copyright holder. To view a copy of this licence, visit <http://creativecommons.org/licenses/by/4.0/>.

References

- Liu L, He B, Huang M. The role of transformation-induced plasticity in the development of advanced high strength steels. *Adv Eng Mater*. 2018;20:1701083. <https://doi.org/10.1002/adem.201701083>.
- Beladi H, Tari V, Timokhina IB, Rollett AD, Hodgson PD. On the crystallographic characteristics of nanobainitic steel. *Acta Mater*. 2017;127:426–37. <https://doi.org/10.1016/j.actamat.2017.01.058>.
- Garcia-Mateo C, Caballero FG, Sourmail T, Kuntz M, Cornide J, Smanio V, Elvira R. Tensile behaviour of a nanocrystalline bainitic steel containing 3 wt% silicon. *Mater Sci Eng A*. 2012;549:185–92. <https://doi.org/10.1016/j.msea.2012.04.031>.
- Qian L, Zhou Q, Zhang F, Zhang M, Tian Y. Microstructure and mechanical properties of a low carbon carbide-free bainitic steel co-alloyed with Al and Si. *Mater Des*. 2012;39:264–8. <https://doi.org/10.1016/j.matdes.2012.02.053>.
- Soliman M, Palkowski H. Development of the low temperature bainite. *Arch Civil Mech Eng*. 2016;16:403–12. <https://doi.org/10.1016/j.acme.2016.02.007>.
- Kumar A, Singh A. Mechanical properties of nanostructured bainitic steels. *Materialia*. 2021;15:101034. <https://doi.org/10.1016/j.mtla.2021.101034>.
- Węglowski S, Marcisz J, Garbarz B. Technological properties and applications of high-carbon nanobainitic steels. *Biul Inst Spaw*. 2018;3:29–43. <https://doi.org/10.17729/ebis.2018.3/3>.
- Zhang F, Yang Z. Development of and perspective on high-performance nanostructured bainitic bearing steel. *Engineering*. 2019;5:319–28. <https://doi.org/10.1016/j.eng.2018.11.024>.
- Caballero FG, Bhadeshia HKDH, Mawella KJA, Jones DG, Brown P. Very strong low temperature bainite. *Mater Sci Technol*. 2002;18:279–84. <https://doi.org/10.1179/026708301225000725>.
- Bhadeshia HKDH. Nanostructured bainite. *Proc R Soc A*. 2010;466:3–18. <https://doi.org/10.1098/rspa.2009.0407>.
- Garcia-Mateo C, Caballero FG, Bhadeshia HKDH. Development of Hard Bainite. *SIJ Int*. 2003;43:1238–43. <https://doi.org/10.2355/isijinternational.43.1238>.
- Chang H-T, Yen H-W, Lin W-T, Huang C-Y, Yang J-R. Heat treatment of superbainitic steels. *Int Heat Treat Surf Eng*. 2013;7:8–15. <https://doi.org/10.1179/1749514813Z.00000000048>.
- Hu F, Wu K. Isothermal transformation of low temperature super bainite. *Adv Mater Res*. 2011;146–147:1843–8. <https://doi.org/10.4028/www.scientific.net/AMR.146-147.1843>.
- Singh K, Kumar A, Singh A. Effect of prior austenite grain size on the morphology of nano-bainitic steels. *Metall Mater Trans A*. 2018;49:1348–54. <https://doi.org/10.1007/s11661-018-4492-8>.
- Zhao J, Li J, Ji H, Wang T. Effect of austenitising temperature on mechanical properties of nanostructured bainitic steel. *Materials*. 2017;10:874. <https://doi.org/10.3390/ma10080874>.
- Gong W, Tomota Y, Harjo S, Su YH, Aizawa K. Effect of prior martensite on bainite transformation in nanobainite steel. *Acta Mater*. 2015;85:243–9. <https://doi.org/10.1016/j.actamat.2014.11.029>.
- Yu X-P, Wu H-B, Gu Y, Yuan R, Zhang Y-Y, Feng Y-H. Effect of prior martensite on bainite transformation and microstructure of high-carbon nano-bainitic steel. *J Iron Steel Res Int*. 2022;29:647–54. <https://doi.org/10.1007/s42243-021-00591-5>.
- Hu F, Wu K-M, Zheng H. Influence of Co and Al on bainitic transformation in super bainitic steels. *Steel Res Int*. 2013;84:1060–5. <https://doi.org/10.1002/srin.201200334>.
- Yang J, Qiu H, Xu P, Yu H, Wang Y. The substitution of aluminum for cobalt in nanostructured bainitic steels. *AIP Conf Proc*. 2018. <https://doi.org/10.1063/1.5041096>.
- Eres-Castellanos FGC, Garcia-Mateo C. Stress or strain induced martensitic and bainitic transformations during ausforming processes. *Acta Mater*. 2020;189:60–72. <https://doi.org/10.1016/j.actamat.2020.03.002>.
- Bhadeshia HKDH. Effect of stress and strain on formation of bainite in steels. In: *Hot Workability of Steels and Light Alloys-Composites*, 1996, pp. 543–56.
- Bhadeshia HKDH. Bainite in steel: theory and practice. 3rd ed. Institute of Materials Minerals & Mining; 2015. p. 208–36.
- Hase K, Garcia-Mateo C, Bhadeshia HKDH. Bainite formation influenced by large stress. *Mater Sci Technol*. 2004;12:1499–505. <https://doi.org/10.1179/026708304X6130>.
- Eres-Castellanos A, Garcia-Mateo C, Caballero FG. Future trends on displacive stress and strain induced transformations in steels. *Metals*. 2021;11:1–19. <https://doi.org/10.3390/met11020299>.
- Hu H, Zurob HS, Xu G, Embury D, Purdy GR. New insights to the effects of ausforming on the bainitic transformation. *Mater Sci Eng A*. 2015;626:34–40. <https://doi.org/10.1016/j.msea.2014.12.043>.
- Shipway PH, Bhadeshia HKDH. The effect of small stresses on the kinetics of the bainite transformation. *Mater Sci Eng A*. 1995;201:143–9. [https://doi.org/10.1016/0921-5093\(95\)09769-4](https://doi.org/10.1016/0921-5093(95)09769-4).
- Chang LC, Bhadeshia HKDH. Stress-affected transformation to lower bainite. *J Mater Sci*. 1996;31:2145–8. <https://doi.org/10.1007/BF00356638>.
- Zhou M, Xu G, Hu H, Yuan Q, Tian J. Comprehensive analysis on the effects of different stress states on the bainitic transformation. *Mater Sci Eng A*. 2017;704:427–33. <https://doi.org/10.1016/j.msea.2017.08.013>.
- Zhou M, Xu G, Hu H, Yuan Q, Tian J. Kinetics model of bainitic transformation with stress. *Met Mater Int*. 2018;24:28–34. <https://doi.org/10.1007/s12540-017-7261-0>.
- Gong W, Tomota Y, Koo MS, Adachi Y. Effect of ausforming on nanobainite steel. *Scr Mater*. 2010;63:819–22. <https://doi.org/10.1016/j.scriptamat.2010.06.024>.
- Holzweissig MJ, Canadinc D, Maier HJ. In-situ characterization of transformation plasticity during an isothermal austenite-to-bainite phase transformation. *Mater Charact*. 2012;65:100–8. <https://doi.org/10.1016/j.matchar.2012.01.007>.
- Liu M, Ma Y, Xu G, Zhou M, Zhang X. Effects of plastic stress on transformation plasticity and microstructure of a carbide-free bainite steel. *Metallogr Microstruct Anal*. 2019;8:159–66. <https://doi.org/10.1007/s13632-019-00527-2>.
- Zhou M, Xu G, Wang L, Yuan Q. The varying effects of uniaxial compressive stress on the bainitic transformation under different austenitization temperatures. *Metals*. 2016;6:109. <https://doi.org/10.3390/met6050119>.
- Fischer FD, Reisner G, Werner E, Tanaka K, Caillaud G, Antretter T. A new view on transformation induced plasticity (TRIP). *Int J Plast*. 2000;16:723–48. [https://doi.org/10.1016/S0749-6419\(99\)00078-9](https://doi.org/10.1016/S0749-6419(99)00078-9).
- Greenwood GW, Johnson RH. The deformation of metals under small stresses during phase transformations. *Proc R Soc Lond Ser A*. 1965;283:403–22. <https://doi.org/10.1098/rspa.1965.0029>.
- Hu H, Xu G, Dai F, Tian J, Chen G. Critical ausforming temperature to promote isothermal bainitic transformation in prior-deformed austenite. *Mater Sci Technol*. 2019;35:420–8. <https://doi.org/10.1080/02670836.2019.1567663>.

37. Eres-Castellanos A, Morales-Rivas L, Latz A, Caballero FG, Garcia-Mateo C. Effect of ausforming on the anisotropy of low temperature bainitic transformation. *Mater Charact.* 2018;145:371–80. <https://doi.org/10.1016/j.matchar.2018.08.062>.
38. Garcia-Mateo C, Jimenez JA, Lopez-Ezquerria B, Rementeria R, Morales-Rivas L, Kuntz M, Caballero FG. Analyzing the scale of the bainitic ferrite plates by XRD. *SEM TEM Mater Charact.* 2016;122:83–9. <https://doi.org/10.1016/j.matchar.2016.10.023>.
39. Chulist R, Czaja P. On the role of atomic shuffling in the 40, 4M and 8M martensite structures in Ni-Mn-Sn single crystal. *Scr Mater.* 2020;189:106–11. <https://doi.org/10.1016/j.scriptamat.2020.08.007>.
40. Wojcik A, Chulist R, Czaja P, Kowalczyk M, Zackiewicz P, Schell N, Maziarz W. Evolution of microstructure and crystallographic texture of Ni-Mn-Ga melt-spun ribbons exhibiting 115% magnetic field-induced strain. *Acta Mater.* 2021;219:117237. <https://doi.org/10.1016/j.actamat.2021.117237>.
41. Alawadhi MY, Sabbaghianrad S, Huang Y, Langdon TG. Direct influence of recovery behaviour on mechanical properties in oxygen-free copper processed using different SPD techniques: HPT and ECAP. *J Mark Res.* 2017;6:369–77. <https://doi.org/10.1016/j.jmrt.2017.05.005>.
42. He J, Du J, Zhang W, Zhang C, Yang Z-G, Chen H. Abnormal anisotropic dilatation during bainitic transformation of ausformed austenite. *Metall Mater Trans A.* 2019;50A:540–6. <https://doi.org/10.1007/s11661-018-5038-9>.
43. Zhou M-X, Xu G, Wang L, Xue Z-L, Hu H-J. Comprehensive analysis of the dilatation during bainitic transformation under stress. *Met Mater Int.* 2015;21:985–90. <https://doi.org/10.1007/s12540-015-2348-y>.
44. Santajuana MA, Eres-Castellanos A, Ruiz-Jimenez V, Allain S, Geandier G, Caballero FG, Garcia-Mateo C. Quantitative assessment of the time to end bainitic transformation. *Metals.* 2019;9:925. <https://doi.org/10.3390/met9090925>.
45. Trzaska J. Empirical formulae for the calculation of austenite supercooled transformation temperatures. *Arch Metall Mater.* 2015;60:181–5. <https://doi.org/10.1515/amm-2015-0029>.
46. Xiong XC, Chen B, Huang MX, Wang JF, Wang L. The effect of morphology on the stability of retained austenite in a quenched and partitioned steel. *Scr Mater.* 2013;68:321–4. <https://doi.org/10.1016/j.scriptamat.2012.11.003>.
47. Wang X, Liu C, Qin Y, Li Y, Yang Z, Long X, Wang M, Zhang F. Effect of tempering temperature on microstructure and mechanical properties of nanostructured bainitic steel. *Mater Sci Eng A.* 2022;832: 142357. <https://doi.org/10.1016/j.msea.2021.142357>.
48. Gong W, Tomota Y, Adachi Y, Paradowska AM, Kelleher JF, Zhang SY. Effects of ausforming temperature on bainite transformation, microstructure and variant selection in nanobainite steel. *Acta Mater.* 2013;61:4142–54. <https://doi.org/10.1016/j.actamat.2013.03.041>.
49. Garcia-Mateo C, Caballero FG. The role of retained austenite on tensile properties of steels with bainitic microstructures. *Mater Trans.* 2005;46:1839–46. <https://doi.org/10.2320/matertrans.46.1839>.
50. Rementeria R, Morales-Rivas L, Kuntz M, Garcia-Mateo C, Kersch E, Sourmail T, Caballero FG. On the role of microstructure in governing the fatigue behaviour of nanostructured bainitic steels. *Mater Sci Eng A.* 2015;630:71–7. <https://doi.org/10.1016/j.msea.2015.02.016>.
51. Nolze G. Improved determination of fcc/bcc orientation relationships by use of high-indexed pole figures. *Cryst Res Technol.* 2006;41:72–7. <https://doi.org/10.1002/crat.200410533>.
52. Beladi H, Adachi Y, Timokhina I, Hodgson PD. Crystallographic analysis of nanobainitic steels. *Scripta Mater.* 2009;60:455–8. <https://doi.org/10.1016/j.scriptamat.2008.11.030>.
53. Matsuzaki A, Bhadeshia HKDH, Harada H. Stress affected bainitic transformation in a Fe–C–Si–Mn alloy. *Acta Metall et Mater.* 1994;42:1081–90. [https://doi.org/10.1016/0956-7151\(94\)90125-2](https://doi.org/10.1016/0956-7151(94)90125-2).
54. Holzweissig MJ, Canadinc D, Maier HJ. In situ characterization of backstress effects on the austenite-to-bainite phase transformation. *Scripta Mater.* 2012;67:368–71. <https://doi.org/10.1016/j.scriptamat.2012.05.027>.
55. Kozeschnik E, Bhadeshia HKDH. Influence of silicon on cementite precipitation in steels. *Mater Sci Technol.* 2008;24:343–7. <https://doi.org/10.1179/174328408X275973>.
56. Beladi H, Timokhina IB, Hodgson PD, Adachi Y. Characterization of nano-structured bainitic steel. *Int J Mod Phys.* 2012;5:1–8. <https://doi.org/10.1142/S2010194512001778>.
57. He SH, He BB, Zhu KY, Huang MX. On the correlation among dislocation density, lath thickness and yield stress of bainite. *Acta Mater.* 2017;135:382–9. <https://doi.org/10.1016/j.actamat.2017.06.050>.
58. Avishan B, Garcia-Mateo C, Morales-Rivas L, Yazdani S, Caballero FG. Strengthening and mechanical stability mechanisms in nanostructured bainite. *J Mater Sci.* 2013;48:61216132. <https://doi.org/10.1007/s10853-013-7408-4>.
59. Olson GB, Cohen M. A mechanism for the strain-induced nucleation of martensitic transformations. *J Less-Common Met.* 1972;28:107–18. [https://doi.org/10.1016/0022-5088\(72\)90173-7](https://doi.org/10.1016/0022-5088(72)90173-7).
60. Zhou Q, Qian L, Tan J, Meng J, Zhang F. Inconsistent effects of mechanical stability of retained austenite on ductility and toughness of transformation-induced plasticity steels. *Mater Sci Eng A.* 2013;578:370–6. <https://doi.org/10.1016/j.msea.2013.04.096>.
61. Gao G, Zhang H, Gui X, Tan Z, Bai B, Weng Y. Enhanced strain hardening capacity in a lean alloy steel treated by a “disturbed” bainitic austempering process. *Acta Mater.* 2015;101:31–9. <https://doi.org/10.1016/j.actamat.2015.08.071>.
62. Allain S, Chateau J-P, Bouaziz O, Migot S, Guelton N. Correlations between the calculated stacking fault energy and the plasticity mechanisms in Fe–Mn–C alloys. *Mater Sci Eng A.* 2004;387–389:158–62. <https://doi.org/10.1016/j.msea.2004.01.059>.
63. Xing X, Zhou Y, Yu H, Liu L, Zhang L, Yang Q. Shear band and α' -martensite induced by stress in laser melting carbide-free bainite layer. *Mater Sci Eng A.* 2018;738:367–74. <https://doi.org/10.1016/j.msea.2018.09.103>.
64. Gao G, Wan K, Su H, Gui X, Li Z, Misra RDK, Bai B. The potential of mechanical twinning in ultrafine retained austenite to enhance high cycle fatigue property of advanced bainitic steels. *Int J Fatigue.* 2020;139: 105804. <https://doi.org/10.1016/j.ijfatigue.2020.105804>.
65. Poddar D, Ghosh C, Bhattacharya B, Singh VK. Development of high ductile ultra high strength structural steel through stabilization of retained austenite and stacking fault. *Mater Sci Eng A.* 2019;762: 138079. <https://doi.org/10.1016/j.msea.2019.138079>.
66. Dao M, Lu L, Shen YF, Suresh S. Strength, strain-rate sensitivity and ductility of copper with nanoscale twins. *Acta Mater.* 2006;54:5421–32. <https://doi.org/10.1016/j.actamat.2006.06.062>.
67. Curtze S, Kuokkala V-T. Dependence of tensile deformation behavior of TWIP steels on stacking fault energy, temperature and strain rate. *Acta Mater.* 2010;58:5129–41. <https://doi.org/10.1016/j.actamat.2010.05.049>.

68. Shen YF, Wang YD, Liu XP, Sun X, Peng RL, Zhang SY, Zuo L, Liaw PK. Deformation mechanisms of a 20Mn TWIP steel investigated by in situ neutron diffraction and TEM. *Acta Mater.* 2013;61:6093–106. <https://doi.org/10.1016/j.actamat.2013.06.051>.
69. Avishan B, Yazdani S, Caballero FG, Wang TS, Garcia-Mateo C. Characterisation of microstructure and mechanical properties in two different nanostructured bainitic steels. *Mater Sci Technol (UK)*. 2015;31:1508–20. <https://doi.org/10.1179/1743284714Y.0000000745>.
70. Hassan HS, Peet MJ, Avettand-Fènoël M-N, Bhadeshia HKDH. Effect of tempering upon the tensile properties of a nanostructured bainitic steel. *Mater Sci Eng A*. 2014;615:340–7. <https://doi.org/10.1016/j.msea.2014.07.097>.
71. Zhao J, Lv B, Zhang F, Yang Z, Qian L, Chen C, Long X. Effects of austempering temperature on bainitic microstructure and mechanical properties of a high-C high-Si steel. *Mater Sci Eng A*. 2019;742:179–89. <https://doi.org/10.1016/j.msea.2018.11.004>.
72. Garcia-Mateo C, Caballero FG, Chao J, Capdevila C, Garcia De Andres C. Mechanical stability of retained austenite during plastic deformation of super high strength carbide free bainitic steels. *J Mater Sci*. 2009;44:4617–24. <https://doi.org/10.1007/s10853-009-3704-4>.

Publisher's Note Springer Nature remains neutral with regard to jurisdictional claims in published maps and institutional affiliations.